Influence of strain rate and temperature on the onset of strain induced crystallization in natural rubber

*Nicolas Candau [a,b], Rabia Laghmach [b,c], Laurent Chazeau *[,a,b], Jean-Marc Chenal [a,b], Catherine Gauthier [d], Thierry Biben [c], Etienne Munch [d]*

[a]Université de Lyon, CNRS, France

[b]MATEIS, INSA-Lyon, CNRS UMR5510, F-69621, France

[c]Institut Lumière Matière, UMR5306 CNRS, Université Claude Bernard Lyon 1, 69622 Villeurbanne Cedex, France

[d]Manufacture Française des Pneumatiques Michelin, Centre de technologies, 63040 Clermont Ferrand Cedex 9, France

*Corresponding author: Laurent Chazeau, e-mail: laurent.chazeau@insa-lyon.fr

KEYWORDS: strain induced crystallization, natural rubber, in situ WAXS

Abstract

Strain induced crystallization (SIC) of natural rubber (NR) has been studied in a large range of strain rate (from 5.6×10^{-5} s^{-1} to 2.8×10^{1} s^{-1}) and temperature (from -40°C to 80°C) combining mechanical and thermal analysis. Both methods are used to extend the study of SIC from slow strain rates – basically performed with in situ wide angle X-rays scattering (WAXS) – to high

strain rates. Whatever the temperature tested, the stretching ratio at crystallization onset (λ_c) increases when the strain rate increases. This strain rate effect is strong at low temperature (close to T_g) and weak at high temperature (much higher than T_g). A theoretical approach derived from the Hoffman-Lauritzen equation has been developed and provides a good qualitative description of the experimental results. At low temperature, the strong increase of λ_c with strain rate is explained by a too long diffusion time compared to the experimental time. At high temperature, SIC kinetics is rather controlled by the nucleation barrier. When the stretching ratio increases due to strain rate effects, this nucleation barrier strongly decreases, allowing crystallization even for short experimental time.

1. Introduction

Most of the studies devoted to strain induced crystallization (SIC) are performed in so-called "quasi-static" conditions: they are carried out at sufficiently low strain rates to lead to a crystallization level which is roughly stable, at a given stretching ratio, over a time range of the order of the experimental time. Such experiments represent the main contribution of the literature to the study of SIC [1-10]. Nevertheless, the dynamic character of SIC in vulcanized natural rubber (NR) [11, 12] was evidenced few years after its discovery in 1925 [13]. It was shown that SIC of NR requires only very short time to occur, as soon as the stretching ratio is high enough. Several studies have also analyzed the stretching ratio at the crystallization onset λ_c as a function of the strain rate. It was shown an increase of this parameter with the strain rate for NR [5], IR (isoprene rubber) [14] or filled NR [15]. Thanks to in situ WAXS measurements [16] or through infra-red analysis [17], the shortest time needed for the appearance of SIC is around several decades of milliseconds for a sample of NR stretched at a stretching ratio of 5, at room temperature (more details on these pioneering works are given in a recent review [18]). This range of induction time was confirmed by

recent in situ WAXS experiments using the stroboscopic technique [19, 20] or impact tensile test [21, 22]. However, in spite of a large number of experimental investigations, a question remains unsolved: what are the physical parameters that control SIC kinetics? This question is important in order to properly describe this phenomenon. It is also essential for rubber applications, where the material is submitted to dynamic strain over an extremely large frequency range. Moreover, it is noteworthy that there is no study presenting SIC over a sufficiently large strain rate and temperature ranges allowing a good description of this phenomenon.

Thus, this work presents a SIC study over a strain rates range of around six decades. This is made possible by combining several experimental techniques of detection such as WAXS analysis, mechanical and thermal characterizations. In order to clarify the respective contributions of nucleation and diffusion in the SIC kinetics, the combined effects of temperature (from -40°C to 80°C) and strain rates is also investigated. These contributions are finally quantified through a Hoffman-Lauritzen type description adapted to SIC. This approach is partly based on a thermodynamic development presented in previous papers [23, 24]. It is coupled in the present study with the WLF diffusion equation. This approach provides a theoretical frame capable of explaining how temperature and strain influence the appearance of SIC in natural rubber.

2. Material and experiments

2.1. Materials

The studied material is a vulcanized unfilled natural rubber. The material recipe is the following: rubber gum (100 phr) which is a Technically Specified Rubber (TSR20) provided by Michelin Tire Company, stearic acid (2 phr), ZnO (1.5 phr), 6PPD (3 phr), CBS (1.9 phr) and sulfur (1.2 phr) (where phr means g per 100 g of rubber). The material has been processed following the

Rauline patent [25]. First, the gum is introduced in an internal mixer and sheared for 2 min at 60°C. Then, the vulcanization recipe is added and the mix is sheared for 5 min. Afterward, the material is sheared in an open mill for five minutes at 60°C. Sample sheets are then obtained by hot pressing at 170°C during 13 min. Dumbbell-shaped samples, with a 6 mm gauge length (l_0) and 0.8 mm thickness, are machined. The number density of the elastically effective sub-chains (so-called hereafter average network chain density ν) was estimated from the swelling ratio in toluene and from the Flory – Rehner equation [26] and found equal to 1.4×10^{-4} mol.cm^{-3}. This density is tuned so that (i) it promotes the development of strain induced crystallization [4] and (ii) it is high enough to avoid an inverse yield effect [27]. In order to avoid microstructure modification during the different mechanical tests, i.e. an uncontrolled Mullins effect, the samples are stretched four times up to stretching ratio ($\lambda = 7$) higher than the maximum stretching ratio reached during the in situ cyclic tests ($\lambda = 6$). A similar procedure is proposed in the work of Chenal et al.[4]

2.2. In situ WAXS

The in situ WAXS experiments are carried out on the D2AM beamline of the European Synchrotron Radiation Facility (ESRF). The X-ray wavelength is 1.54 Å. Because of a limitation due to the relatively long detection times (several seconds) of the CCD camera, in situ WAXS are only performed at low strain rates (4.2×10^{-3} s^{-1} and 1.7×10^{-2} s^{-1}). For the lowest speed, the sample is tested through a monotonic loading-unloading cycle. For the highest ones, the sample is only stretched and then relaxed in the deformed state.

The two-dimensional (2D) WAXS patterns are recorded by a CCD camera (Princeton Instrument). The beam size is small enough (300 µm × 300 µm) to avoid superimposition with the scattered signal. The background, (i.e. air scattering and direct beam intensities) is properly measured in absence of any sample. It can then be subtracted to the total intensity scattered in the

presence of the rubber sample. The corrected scattering intensity is finally normalized by the thickness and the absorption of the sample. Each scattering pattern is integrated azimuthally. The deconvolution of the curve $I=f(2\theta)$ enables the extraction of the intensity at the peak top and the width at half height of each crystalline peak and the intensity at the peak top of the amorphous phase. The crystallinity index CI is then calculated as follows [28]:

$$\frac{I_{a0} - I_{a\lambda}}{I_{a0}} \quad (1)$$

where I_{a0} and $I_{a\lambda}$ are the intensity of the amorphous phase at the peak top in the unstretched state and the stretched state, respectively.

2.3 Mechanical characterization

The EPLEXOR® 500 N of Gabo Qualimeter society (Ahlden**,** Germany) is used in order to carry out mechanical characterization at different temperatures. Mechanical tests consist of a monotonic stretching at various strain rates, from 5.6×10^{-5} s^{-1} to 1.1×10^{-1} s^{-1} and from the relaxed state up to the maximum stretching ratio $\lambda = 6$. Before each tensile test, a soak time of five minutes guarantees that the desired temperature (from -40°C to 80°C), obtained by air circulation, is homogeneous in the oven. The test carried out at the lowest strain rate is stopped at an early stage (λ around 5) because the time reaches the limitations of the experimental set up. To perform experiments at highest strain rates, ranging from 1.1×10^{-1} s^{-1} to 2.8×10^{1} s^{-1}, mechanical characterization is carried out thanks to an MTS tensile test machine. For all the mechanical tests, the tensile force is converted into nominal stress $\sigma = F/S_0$. Stress is then plotted as a function of the nominal stretching ratio $\lambda = l/l_0$. λ is accurately measured by videoextensometry.

2.4. Infrared thermography coupled with mechanical tests

For the highest strain rates, ranging from 1.1×10^{-1} s^{-1} to 2.8×10^{1} s^{-1}, coupled mechanical and thermal characterization is carried out thanks to an MTS tensile test machine. Two types of mechanical tests are performed: (i) Stretching/unstretching, (ii) stretching and relaxation in the deformed state. The temperature increase on the samples surface during such tests is measured thanks to an infrared pyrometer (Microepsilon, CTLF-CF3-C3) whose acquisition time is equal to 9 msec.

Obviously, direct deduction of the stretching ratio at SIC onset (λ_c) from the surface temperature variation is pertinent when the sample is not too far from adiabatic conditions. In order to determine the range of the experimental time for which such conditions are respected, a sample is stretched at the maximum strain rate allowed by the device (2.8×10^{1} s^{-1}, i.e. an equivalent stretching time of 0.3 s), and at the maximum stretching ratio ($\lambda = 6$) to induce a maximum temperature variation. The sample is then maintained in the deformed state. Figure 1 presents the evolution of the stress and temperature variation on the sample surface (ΔT equal to T minus 294K) as a function of the time. ΔT strongly increases during the stretching (+3°C). It continues to increase significantly during the very beginning of the relaxation phase (+3°C), i.e. from 0.3 sec to 0.5 sec. During such short times, the stress significantly decreases from 2.75 to 2.55 MPa. The temperature evolution is well explained by an increase of the crystallinity. From 0.5s to 2s, temperature variations slow down and reach a plateau. This suggests that CI still increases but much more slowly. After 2s, temperature decreases down to room temperature. During this time, heat generated by crystallization and accumulated in the sample begins to dissipate in the room. Thus, these 2 seconds are a good estimate of the time below which the adiabatic conditions can be assumed.

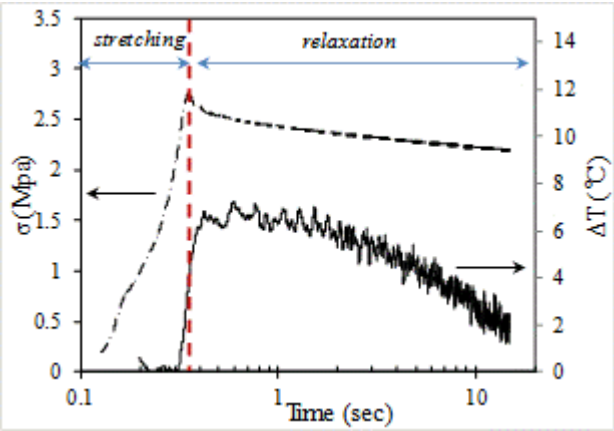

Figure 1. Stress (dash dotted line) and surface temperature variation (solid line) versus time for a sample of NR stretched at room temperature and high strain rate (2.8×10^{1} s^{-1}) and relaxed at λ = 6.

3. Experimental results

3.1. SIC Onset detected by WAXS

We first present SIC phenomenon in common experimental conditions, i.e. a cyclic deformation at room temperature and "slow" strain rate (4.2×10^{-3} s^{-1}). Figure 2 shows the nominal stress and the crystallinity index (CI) plotted as a function of the stretching ratio. In these conditions, the stretching ratio at the SIC onset (λ_c) is around 4.3. Above this value, CI increases and reaches a maximum of 14% at λ equal to 6. From a mechanical point of view, the effect of SIC is twofold. Formation of oriented crystallites first decreases the local stretching ratio of the non-crystallizable chains [5, 8, 14, 29]. Secondly, at higher stretching ratios (λ above 5) the increasing number of crystallites, which may act as new crosslinks, take part to an increase of the local stretching ratio [6]. Although not clear from a thermodynamic point of view, this scheme explains that the stress first decreases and then increases compared to an amorphous rubber. To accurately demonstrate that the hardening effect is related to SIC rather than to the limit extensibility of the

chains, as predicted by the theory of rubber elasticity [30], the stress-strain curve at 21°C is compared to the one of an amorphous NR sample, i.e. stretched at 80°C (see figure 13 in the appendix). After a correction of the entropic effect (the stress of the sample at 80°C is multiplied by the ratio (273+21)/(273+80)), the strong increase of the stress in the crystallized sample clearly shows that the hardening is due to SIC.

During unloading, CI decreases and crystallites totally melt at λ equal to 3, showing an hysteresis curve. The stress-strain curve also exhibits an hysteretic shape and the material recovers its hyper-elastic behaviour at λ equal to 3, i.e. when the last crystallites melt. Because nucleation is a kinetic process involving an energy barrier related to the surface energy of the crystallites, nucleation is delayed and needs an excess stretching ratio to occur; such "superstraining effect" is comparable to the supercooling effect that occurs during thermal crystallization. This explains the observed CI hysteresis. This also means that crystallization strongly depends on the strain rate. The kinetics nature of SIC can also been evidenced by stretching a NR sample at slow strain rate (4.2×10^{-3} s^{-1}) and letting it relax at different stretching ratios (λ = 4.3, 5.3 and 6, cf. figure 2). CI still increases and stress decreases during the relaxation phase (refer to the cross symbols on figure 2). Note that the stress relaxation at λ=6 measured on a totally amorphous sample (i.e. stretched at 80°C) is significantly lower than the one observed on the crystallizing sample (stress is decreased of 0.3 MPa at 21°C and 0.1 MPa at 80°C, unpresented data). This suggests that the stress relaxation observed at 21°C is likely due to SIC. The CI increase during the relaxation step is particularly important for the lowest stretching ratio (λ = 4.3). This means that the stretching ratio at SIC onset is strongly dependent on the experimental time, i.e. on the strain rate. This has been reported in literature [14], and we have also checked that a strain rate difference of less than one decade is enough to lead to a slight increase of λ_c (unpresented data).

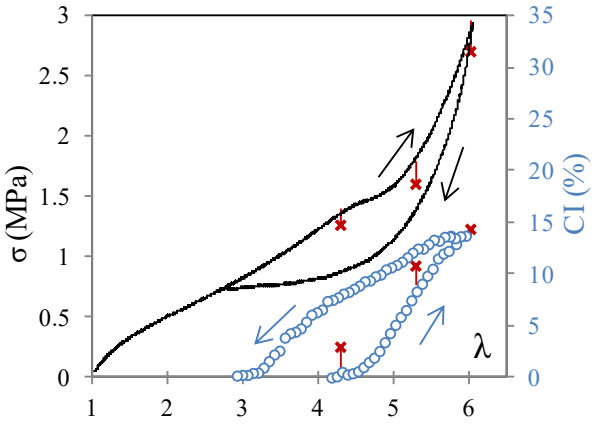

Figure 2. CI (circle symbols) and stress (solid line) versus λ, during a cyclic deformation of NR sample at room temperature, with the strain rate 4.2×10^{-3} s^{-1}. CI and stress values measured after 5 minutes of relaxation on NR samples stretched from $\lambda = 1$ up to $\lambda = 4.3$, 5.3 and 6 at room temperature with the strain rate 4.2×10^{-3} s^{-1} (cross symbols).

3.2. SIC onset detected by mechanical relaxation

In order to observe a more noticeable effect of the strain rate, samples are now stretched at room temperature in a wider range of strain rates (from 5.6×10^{-5} sec^{-1} to 2.8×10^{-1} sec^{-1}). Stress-strain curves (σ-λ) are plotted in figure 3a. As previously mentioned, SIC is associated with a stress relaxation followed by a hardening. The relaxation intensity as well as the hardening are progressively decreased by an increase of the strain rate. This is explained by a lower crystallinity. The stretching ratio associated with the beginning of the mechanical relaxation can be considered as a good estimate of λ_c. It is more accurately deduced from the evolution of the tangent modulus E_t, equal to $d\sigma/d\lambda$, as a function of the stretching ratio (figure 3b). λ_c is estimated as the stretching ratio at which E_t reaches a maximum before the relaxation (see vertical arrow as exemplified in figure 3b for the lowest strain rate), i.e. when its derivative is equal to zero. The mechanical responses corresponding to the previous in situ WAXS experiments are also plotted

(curve 3 and 4). As shown in figure 2 and also in figure 6, a good agreement is found between both methods for the estimate of λ_c. On curve 6 of figure 3b (highest strain rate), the relaxation phenomenon (i.e. decrease of E_t) is not clearly evidenced. Thus, at this strain rate, this method appears to be inappropriate to accurately detect the beginning of SIC. At least, the value of λ_c should be confirmed by a complementary experiment. This can be done by a thermal analysis of SIC process as proposed in the following section.

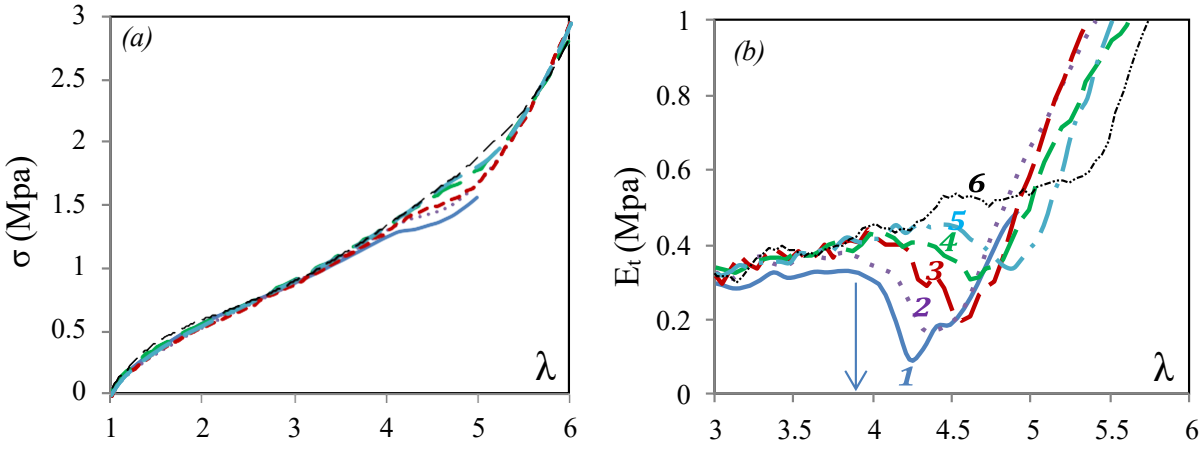

Figure 3. σ-λ curves (a) and E_t-λ curves (b) for different strain rates: 5.6×10^{-5} s^{-1} (1), 4.2×10^{-4} s^{-1} (2), 4.2×10^{-3} s^{-1} (3), 1.7×10^{-2} s^{-1} (4), 1.1×10^{-1} s^{-1} (5) and 2.8×10^{-1} s^{-1} (6). The vertical arrow indicates the value of λ_c for the lowest strain rate.

3.3. SIC onset detected by temperature variation

Crystallization is an exothermic phenomenon and consequently has a thermal signature. Mitchell was the first to study SIC from the temperature variations of the sample surface [17]. A similar approach is used in the present study. Figure 4 presents the evolution of the mechanical and thermal responses of a NR sample stretched and unstretched at 1.4×10^{-1} s^{-1} from $\lambda = 1$ to $\lambda = 6$. The typical correlation between the mechanical and crystalline hysteresis presented in figure 2 is also found between the mechanical and thermal ones: (i) the beginning of the mechanical

relaxation and of the temperature increase are concomitant and (ii) both hysteresis loops close at similar stretching level. Viscoelasticity has only a weak thermal effect compared to crystallization, since as soon as crystallinity has disappeared, both loading and unloading curves are superimposed. This quasi-exclusive contribution of crystallization to the thermal hysteresis was nicely demonstrated in recent works [31, 32].

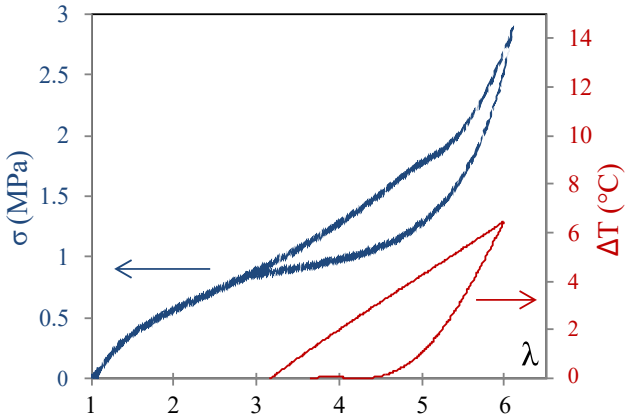

Figure 4. Stress and surface temperature versus stretching ratio for a NR sample stretched and unstretched at 1.4×10^{-1} s^{-1}.

Thermal and mechanical signatures of SIC are now studied for different strain rates during the stretching phase. When the strain rate increases, the stretching ratio at which heating appears is progressively increased (figure 5). In the same way, the maximum heating reached at the maximum stretching ratio is decreased, suggesting a lower crystallization. Taking into account the experimental uncertainties of the measurements, (in terms of stretching ratio, the error bar is +/-0.15 for mechanical tests, +/-0.2 for thermal analysis), the stretching ratios at SIC onset deduced from thermal measurements and from mechanical tests are in good agreement in the range of strain rates tested (figure 14 in the appendix).

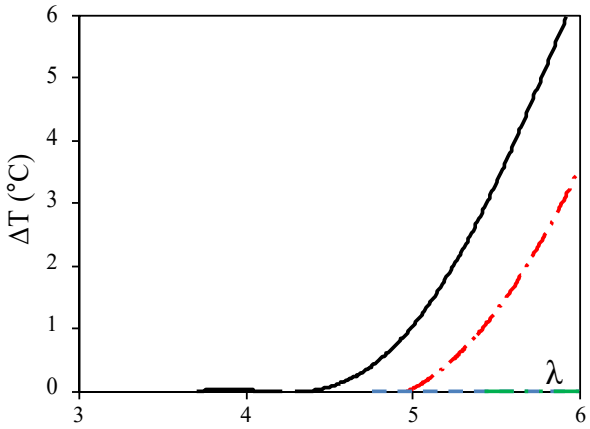

Figure 5. Temperature increase during stretching at different strain rates: $1.1 \times 10^{-1} s^{-1}$ (solid lines), $1.4\ s^{-1}$ (dotted lines), $5.6\ s^{-1}$ (dash dotted lines) and $2.8 \times 10^{1} s^{-1}$ (double dash dotted lines).

3.4. Effect of strain rate on the SIC onset

λ_c extracted from mechanical, thermal and WAXS analysis, are now plotted as a function of the time needed to reach this stretching ratio (calculated as the ratio of (λ_c - 1) by $d\lambda/dt$). This so-called induction time is therefore the time at which SIC appears. As shown in figure 6, above a critical induction time around 10^{3} / 10^{4} sec, SIC is poorly affected by the strain rate. Below it, the stretching ratio at SIC onset is progressively and significantly increased up to a maximum value of 5.6 (for the strain rate range studied). Theoretically, SIC can be delayed due to a delay of the crystallite nucleation, and (or) a delay of crystallite growth. As a first approximation, growth process is assumed instantaneous during stretching at room temperature and strain rates close to quasi-static conditions: SIC is then controlled by the nucleation process, which mainly depends on the stretching ratio. This is consistent with the study of Andrews [33]. One can also wonder what is the role of the diffusion of the macromolecules, which is commonly related to the characteristic time of the α relaxation of the chain segments. This time can be considered as negligible for experiments carried out in quasi-static conditions. However, at high strain rates (stretching times

much lower than $10^3/10^4$ sec) diffusion kinetics might play a role. For a better understanding of this phenomenon, the following paragraph is devoted to the study of the combined effects of temperature and strain rate on SIC kinetics.

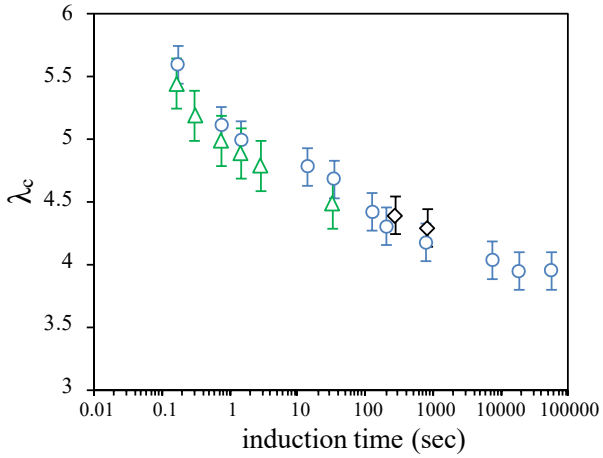

Figure 6. λ_c versus the stretching time deduced from WAXS (diamond symbols), mechanical relaxation (circle symbols) and temperature variations (triangle symbols).

3.5. Combined effects of strain rate and temperature

The effect of the strain rate on λ_c is now studied at different temperatures varying from -40°C to 80°C. λ_c is deduced from tensile tests (cf. method described in section 3.2) for strain rates ranging from 5.6×10^{-5} s^{-1} to 1.1×10^{-1} s^{-1}. The stress is corrected from the temperature effect on the entropic elasticity, through a correcting factor equal to the room temperature over *T*. Similarly to the tests performed at room temperature (figure 3), the evolution of the tangent modulus during loading at -25°C exhibits both relaxation and hardening (figure 7). This is true for the different strain rates, except for the lowest one, for which stress relaxation is not observed whereas hardening effect is stronger and appears at very low stretching ratio. This might be explained by the fact that at such low temperature and stretching ratio, a part of the crystallization is thermally

induced, and thus leads to a high CI content. The Yield effect observed above $\lambda = 2$ is typical of the microstructural modification of the crystalline microstructure of a semi-crystalline polymer during its stretching.

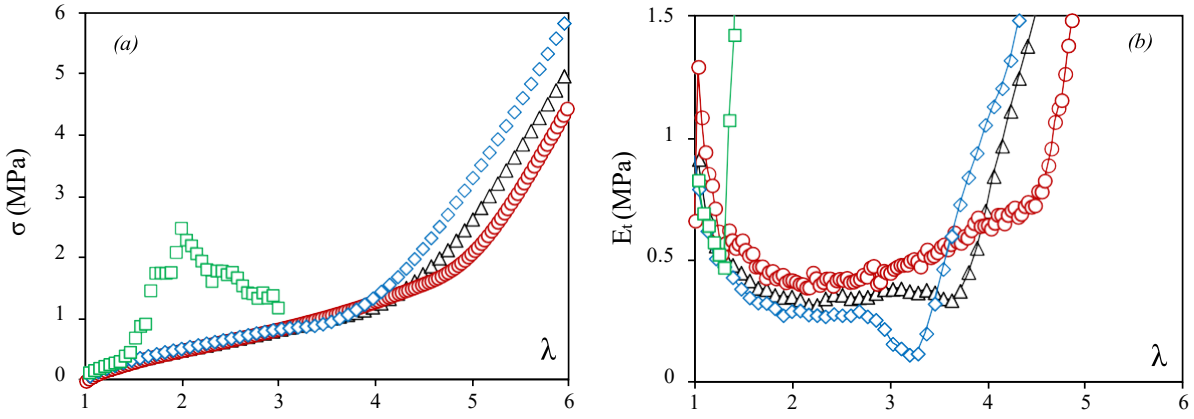

Figure 7. σ (a) and E_t (b) versus λ during stretching at -25°C for different strain rates: 5.6×10^{-5} s^{-1} (square symbols), 4.2×10^{-4} s^{-1} (diamond symbols), 4.2×10^{-3} s^{-1} (triangle symbols) and 1.1×10^{-1} s^{-1}(circle symbols).

For a sufficiently slow strain rate (4.2×10^{-4} s^{-1}), λ_c shows a minimum value at -25°C (cf. figure 8). This is consistent with the study of Toki et al. [1] in which NR samples are stretched in similar experimental conditions. This temperature is often reported to be the one at which crystallization is the fastest, for unstretched polyisoprene rubber (natural or synthetic) in the undeformed state [34-36]. This is then explained by the antagonistic effects of an easier chains diffusion at high temperature (much higher than the glass transition temperature T_g), and of an easier nucleus formation at low temperature (much lower than the equilibrium melting temperature T_m).

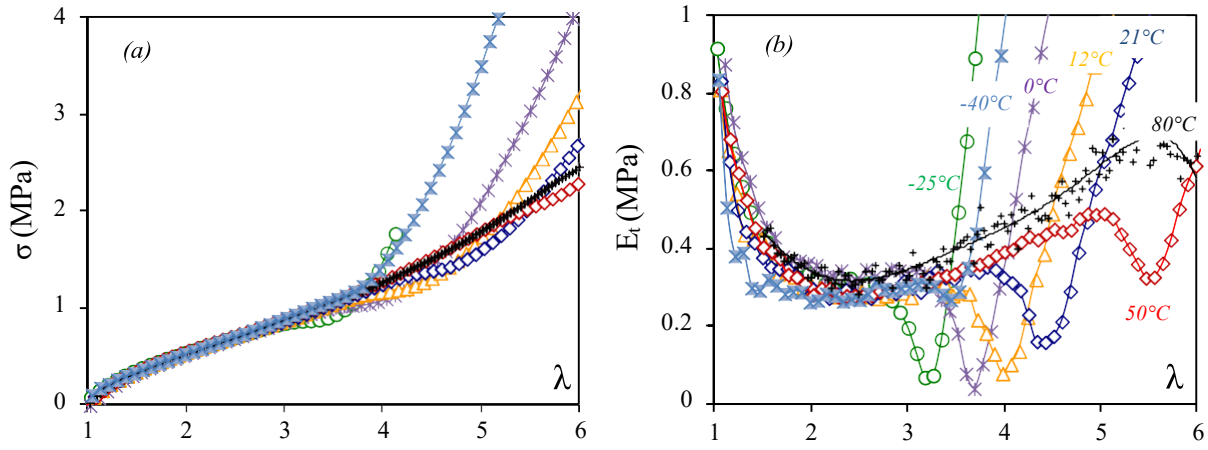

Figure 8. (a) Stress and (b) tangent modulus as a function of the stretching ratio during stretching performed at 4.2×10^{-4} s^{-1} and temperatures varying from -40°C to 80°C.

The evolution of λ_c with temperature is plotted in figure 9 for different strain rates (4.2×10^{-4} s^{-1}, 1.7×10^{-2} s^{-1} and 1.1×10^{-1} s^{-1}). All curves show a minimum λ_c value for a temperature for which crystallization is therefore the easiest. This temperature increases from -25°C to 0°C with the strain rate. This is likely explained by the fact that diffusion and nucleation rates are not identically affected by temperature and stretching ratio. For the lowest temperatures (closest to the glass transition), when the strain rate increases, λ_c is strongly increased because the chains need more time to diffuse. For the highest temperatures, at which diffusion is eased, strain rate effects are smaller. In these conditions, SIC is rather limited by a too long nucleation time, i.e. a too high nucleation barrier energy. Now, when the stretching ratio increases due to strain rate effects, this nucleation energy barrier decreases. Thus, SIC can finally occur at high stretching ratio, even for short experimental times, explaining the weak effect of the strain rate on λ_c at high temperature. The dependence of this nucleation barrier and of the chains diffusion on stretching ratio and temperature are quantified in the following discussion.

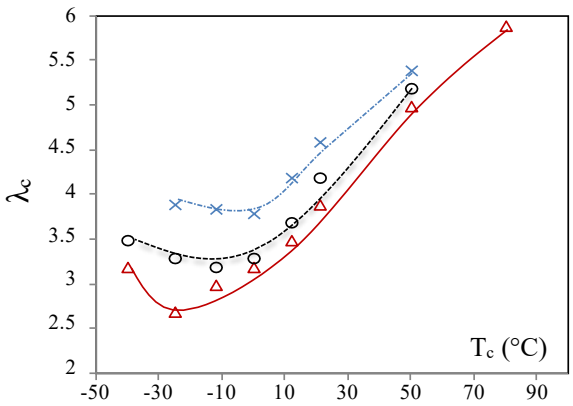

Figure 9. λ_c versus T_c for various strain rates: 4.2×10^{-4} s^{-1} (triangle symbols), 4.2×10^{-3} s^{-1} (circle symbols), and 1.1×10^{-1} s^{-1} (cross symbols). Lines are guides for the eyes.

4. Discussion

According to the theory of phase transition [37], crystallization kinetics depends on the nucleation barrier which needs to be crossed. Because only λ_c is considered here, the energetic formalism for primary nucleation is used (in this description, all crystallites faces are free to grow as no foreign nucleus is pre-existent). Following the theoretical developments of reference 23, the nucleation barrier $\Delta\varphi^*$ can be written:

$$\Delta\varphi^* = \frac{32\sigma^2\sigma_e}{\left[\frac{\nu_1 RT}{2}\left(\lambda_c{}^2 + \frac{2}{\lambda_c} - 3\right) + \Delta H_m \frac{T_{m,\infty} - T}{T_{m,\infty}}\right]^2} \quad (2)$$

Nucleation is eased, i.e. $\Delta\varphi^*$ is lowered, when surface energies are low and when the entropic energy term (or strain energy) and the enthalpic term (which depends on the melting temperature of the infinite crystal) are high. ΔH_m is the melting enthalpy ($\Delta H_m = 6.1 \times 10^7$ $J.m^{-3}$ [38]), $T_{m,\infty}$ is the melting temperature of the infinite crystal in the undeformed state ($T_{m,\infty} = 35.5°C$ [39]), R (8.314 $J.mol^{-1}.K^{-1}$) is the constant of the perfect gazes. $\sigma_l = 0.0033$ $J.m^{-2}$ and $\sigma_e = 0.0066$ $J.m^{-2}$ are the

lateral and chain end surface energies. Their values are deduced from the Thomas-Stavley relationship [40] and from the assumption that σ_e is almost equal to twice σ_l, as proposed in a previous work [23]. As a first approximation, given the fact that only the SIC onset will be discussed here, the expression of the strain energy neglects the limit extensibility of the chains [41, 42]. A special attention is given to the estimate of ν_1, the network density of the first chains involved in SIC (in mol.cm^{-3}). One of the basic interpretations of SIC phenomenon, first proposed by Toki [43] and Tosaka [44], is to consider that highly stretched molecules, i.e. the shortest ones, are the first that nucleate. This is consistent with strong heterogeneity of the crosslink density in NR sample. In a previous study [23], we developed an approach following this point of view, and estimated the value of the network chain density of the first molecules involved in SIC process ($\nu_1 \sim 4.1 \times 10^{-4}$ mol.cm^{-3}).

The nucleation probability N_1 can be estimated with a Boltzmann's type equation:

$$N_1 \propto \exp\left(\frac{-\Delta\varphi^*}{k_B T}\right) \tag{3}$$

$k_B = R/N_a$ is the Boltzmann constant and N_a the Avogadro constant. The crystallization rate is then defined as follows [14, 40]:

$$\dot{N} = \dot{N}_0 D_1 N_1 \tag{4}$$

Where $\dot{N}_0$ is approximated as a constant (although it should depend on 1/T), D_1 is a diffusion (or transport) term derived from WLF equation.[45] This empirical relationship allows estimating the dependence of the relaxation time with temperature, when this one is above the glass transition temperature T_g. D_1 can be written:

$$D_1 = \exp\left(\frac{-2.0303 C_1 C_2}{C_2 + T - T_g}\right) \quad (5)$$

The diffusion term is not equal but proportional to the exponential term. Actually, this coefficient is included in the global pre-factor $\dot{N}_0$. Using the time-temperature superposition principle, the shift factor a_T – calculated from the construction of a master curve from mechanical spectrometry data – allows estimating the parameters C_1, C_2 and T_g, that we found equal to 16.8, 33.6 K and 208 K (-65 °C) respectively. The α relaxation of chain segments is not the unique relaxation mode that characterizes the movement of the polyisoprene chain. Note that these parameters were deduced from experiments in the linear regime, i.e. at small strain: we will assume here that the segmental mobility is independent on the stretching ratio.[46] Moreover, the polyisoprene chain of natural [47] or synthetic rubber [48] exhibit a normal mode relaxation associated with the translational motion of the whole chain. Nevertheless, whatever the type of relaxation chosen in the present description, the dependence of the diffusion term with temperature remains the same, because of the assumed proportionality between normal and segmental relaxation times. Within this frame, a plot of $\dot{N}/\dot{N}_0$ versus temperature for different λ shows classical bell-shape curves with a maximum resulting from the increase of the diffusion term D_1 and a decrease of the nucleation term N_1 with temperature (cf. insert in figure 11).

The induction time τ needed to observe crystallization can be roughly estimated from:

$$\tau \propto 1/\left(\dot{N}_0 D_1 N_1\right) \quad (6)$$

For sake of simplicity, in the following discussion, τ will be approximated as the time needed to reach the stretching ratio at SIC onset, during a monotonic experiment at a fixed temperature. In order to fix the time scale of the theoretical curve and enable a comparison with the experimental

data, we arbitrarily choose to estimate N_0, an unknown parameter, from the experimental time τ needed to crystallize the NR sample stretched at the optimum temperature (-25°C) with the lowest strain rate tested, i.e. when λ_c is the lowest. Thus, from the previous equations, the theoretical evolution of the stretching ratio at SIC onset is plotted as a function of the induction time and two studied temperatures (21°C and -25°C) on figure 10. We have also plotted our experimental data obtained at the same temperatures, where the induction time is approximated as the experimental stretching time needed to reach λ_c. Data from the literature performed at different strain rates and room temperature are also reported [7, 8, 15, 17, 44, 49]. Apart for the Mitchell's data [17], they are all obtained from in situ WAXS analysis. For all these studies, the sulphur vulcanized natural rubbers have network chain densities close to the one measured in our sample, explicitly, or implicitly since they have similar chemical composition. The data from the literature are in remarkable agreement with ours. The theoretical curve calculated at -25°C from the thermodynamic approach correctly describes the strong increase of the stretching ratio at crystallization onset measured at -25°C when the strain rate increases.

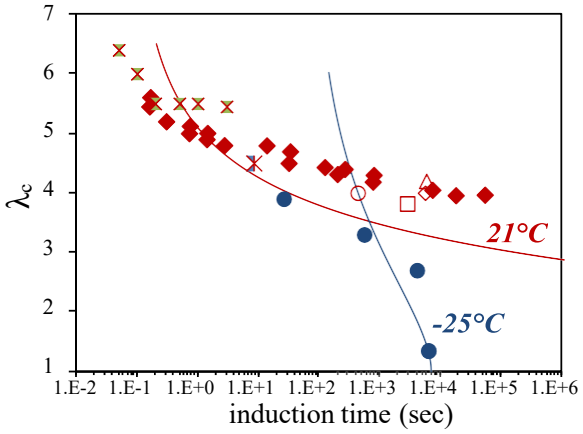

Figure 10. Recall of λ_c values extracted from our own tests at 21°C (filled diamonds) and -25°C (filled circles). Data from literature are added in unfilled symbols: ref. 7 (unfilled circle symbol),

ref. 8 (unfilled triangle symbol), ref. 15 (unfilled diamond symbol), ref. 17 (cross symbols), ref. 44 (double cross symbol), ref. 49 (unfilled square symbol). Predictions of the induction time at 21°C and -25°C deduced from equation 6 (cf. solid lines).

However, the two theoretical curves at -25°C and at room temperature cross each other whereas the experimental data seem to converge when the stretching ratio increases. This means that, at high stretching ratio, the model predicts a too strong increase of τ when the temperature decreases from room temperature to -25°C. This might be due to our questionable assumption of an independence of the diffusion term D_1 on the stretching ratio. Indeed, from equation (6), one can also estimate the time needed to detect crystallization at -25°C in the unstretched state:

$$\tau_0 = 1/\left(\dot{N}_0 D_1\left(T_c = -25°C\right) N_1\left(\lambda = 1, T_c = -25°C\right)\right) \quad (7)$$

τ_0 is found equal to 7000 seconds. This value is more than 15 times lower than the experimental value from the literature.[4] Thus, as said previously, the way we fixed the timescale of the theoretical curve via the value $\dot{N}_0$ is not satisfactory. It however enables to compare on the same graph the experimental data and the theoretical curve calculated at room temperature. Given the strong assumptions chosen for the calculation, the comparison is acceptable and proves the pertinence of our interpretation. An interesting feature of the theoretical curve is its asymptotic evolution at short induction time, which would indicate the existence of a minimum induction time for SIC.

The induction time τ (equation 6) is now plotted in figure 11 as a function of the temperature for different stretching ratios. The influence of the stretching ratio on the induction time is particularly important when temperature is high enough to consider that diffusion is not a limiting

process. In that case, the acceleration of SIC kinetics with λ is due to the increasing contribution of the strain energy, leading to a decrease of the nucleation barrier energy (equation 2). Contrarily, for temperatures close to T_g, all curves converge and describe a slow kinetics because diffusion becomes a limiting parameter for crystallization. Thus, for a given stretching ratio, when varying the temperature, the induction time shows a minimum value, corresponding to the fastest kinetics of crystallization.

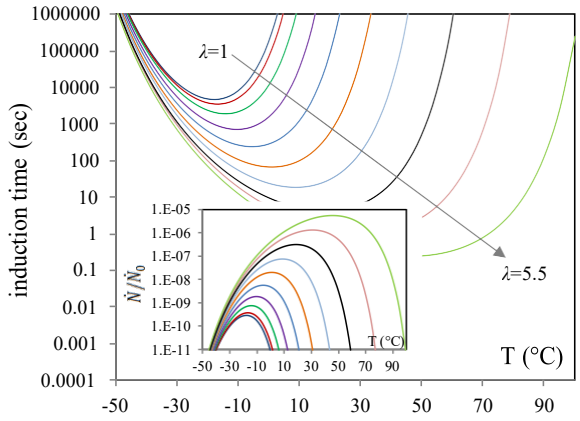

Figure 11. Induction time (τ) versus temperature for stretching ratios varying from $\lambda = 1$ to $\lambda = 5.5$ (between two consecutive plots, $\Delta\lambda = 0.5$). Corresponding normalized rate of crystallization versus temperature (insert).

From these curves, at a given strain rate, i.e. for a given induction time, λ_c can be estimated as a function of the temperature (cf. figure 12). As observed experimentally (cf. figure 9), at a given strain rate, the theoretical curves predict the existence of a minimum λ_c, and that the temperature at this minimum increases with the strain rate. The model also predicts a convergence of the curves at high temperature due to the fact that (i) SIC kinetics is controlled by the nucleation barrier (ii) this energy barrier depends on the strain energy (iii) this strain energy varies rapidly with λ since it depends on λ^2.

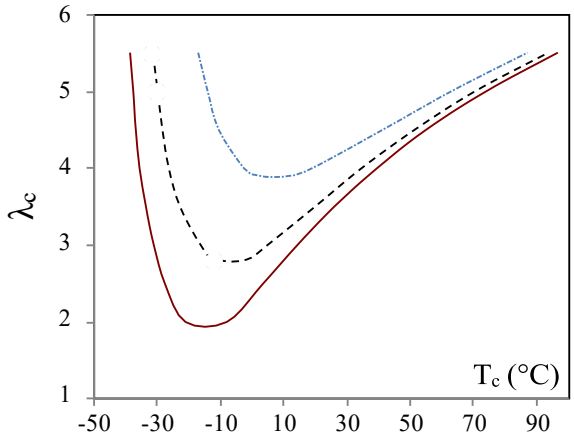

Figure 12. λ_c as a function of the temperature for the three strain rates previously studied (figure 9): 4.2×10^{-4} s^{-1} (solid line), 4.2×10^{-3} s^{-1} (dotted line), and 1.1×10^{-1} s^{-1} (dash dotted line).

5. Conclusion

The combined effects of the strain rate and temperature on the stretching ratio at SIC onset (λ_c) of vulcanized NR have been studied thanks to infrared thermography and mechanical characterization. Both methods allow describing SIC at high strain rates, while in situ wide angle X-rays scattering (WAXS) is only used for slow strain rates. Whatever the temperature tested, λ_c increases when the strain rate increases. Moreover, results show that (i) the temperature at which crystallization is the fastest – so-called optimum temperature – increases when the strain rate increases and (ii) the strain rate effect is particularly important at low temperature (close to T_g) but becomes negligible at high temperatures (much higher than T_g).

To interpret these results, a thermodynamic approach based on the Hoffman-Lauritzen theory allows giving an expression of the induction time needed for crystallization as a function of the stretching ratio and temperature at crystallization onset. This enables a pertinent interpretation of experimental data obtained from both our laboratory and from literature. At low temperature, the strong increase of λ_c with strain rate is likely due to a too long diffusion time compared to the

experimental time. At high temperature, the weak increase of λ_c with strain rate is explained by the fact that SIC kinetics is controlled by the decrease of the nucleation barrier through the rapid increase of the strain energy with the stretching ratio.

However, the relation between molecular movements and SIC characteristic times is not perfectly clear and our results suggest that a contribution of the chain alignment should be included in the expression of their diffusion time. Further investigations correlating WAXS in situ analysis and dielectric measurements should give interesting insights on this question.

6. Acknowledgements

The authors are indebted to the European Synchrotron Radiation Facility (ESRF) and the local contact Dr. C. Rochas for providing the necessary beamline time and technical assistance in the experiments on the D2AM line.

7. Appendix

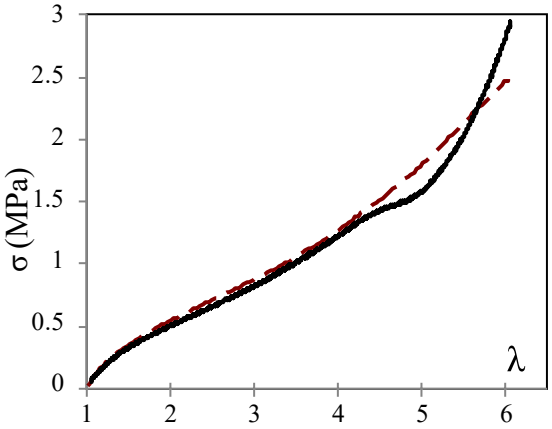

Figure 13. Stress-strain curves of NR sample stretched at room temperature (solid line) and 80°C (dotted line), and at slow strain rate (4.2×10^{-3} s^{-1}).

Figure 14 presents the relation between λ_c extracted from thermal measurements and λ_c deduced

from mechanical tests for different strain rates. One can notice that the data from the mechanical measurement are systematically higher than the values deduced from thermal measurement, This is not surprising because a mechanical signature of the SIC is visible when it begins to compensate the stress increase due to the stretching of the amorphous phase, meaning it needs a significant amount of crystallinity; nevertheless, the overestimate of the mechanical measurement is within the error bar and therefore will be neglected.

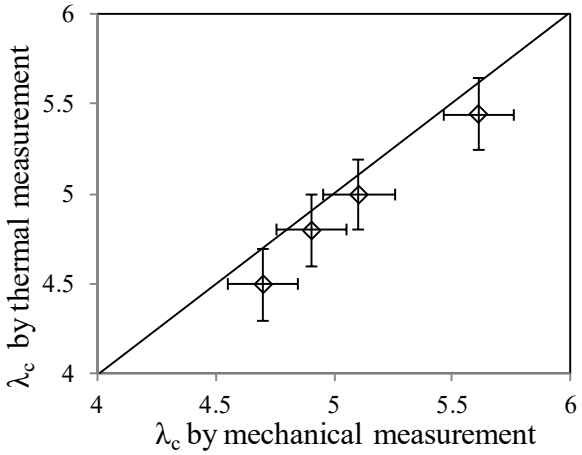

Figure 14. λ_c extracted from thermal measurements versus λ_c from mechanical tests for the strain rates: $1.1 \times 10^{-1} s^{-1}$ (solid lines in insert), $1.4\ s^{-1}$ (dotted lines in insert), $5.6\ s^{-1}$ (dash dotted lines in insert) and $2.8 \times 10^{1} s^{-1}$ (double dash dotted lines in insert).

8. References

1. S. Toki, J. Che, L. Rong, B. S. Hsiao, S. Amnuaypornsri, A. Nimpaiboon and J. Sakdapipanich, Macromolecules 46 (13), 5238-5248 (2013).
2. Y. Ikeda, N. Higashitani, K. Hijikata, Y. Kokubo, Y. Morita, M. Shibayama, N. Osaka, T. Suzuki, H. Endo and S. Kohjiya, Macromolecules 42 (7), 2741-2748 (2009).
3. J. M. Chenal, C. Gauthier, L. Chazeau, L. Guy and Y. Bomal, Polymer 48 (23), 6893-6901 (2007).

4. J. M. Chenal, L. Chazeau, L. Guy, Y. Bomal and C. Gauthier, Polymer 48 (4), 1042-1046 (2007).
5. J. Rault, J. Marchal, P. Judeinstein and P. A. Albouy, Eur. Phys. J. E 21 (3), 243-261 (2006).
6. J. Rault, J. Marchal, P. Judeinstein and P. A. Albouy, Macromolecules 39 (24), 8356-8368 (2006).
7. M. Tosaka, S. Murakami, S. Poompradub, S. Kohjiya, Y. Ikeda, S. Toki, I. Sics and B. S. Hsiao, Macromolecules 37 (9), 3299-3309 (2004).
8. S. Trabelsi, P. A. Albouy and J. Rault, Macromolecules 36 (20), 7624-7639 (2003).
9. S. Toki, T. Fujimaki and M. Okuyama, Polymer 41 (14), 5423-5429 (2000).
10. I. S. Choi and C. M. Roland, Rubber Chem. Technol. 70 (2), 202-210 (1997).
11. J. D. Long, W. E. Singer and W. P. Davey, Industrial and Engineering Chemistry 26, 543-547 (1934).
12. M. F. Acken, W. E. Singer and W. P. Davey, Industrial and Engineering Chemistry 24, 54-57 (1932).
13. J. R. Katz, Naturwissenschaften 13, 410-416 (1925).
14. Y. Miyamoto, H. Yamao and K. Sekimoto, Macromolecules 36 (17), 6462-6471 (2003).
15. S. Beurrot-Borgarino, Thesis, Ecole centrale de Nantes-ECN, Nantes, France, 2012.
16. D. J. Dunning and P. J. Pennells, Rubber Chem. Technol. 40 (5), 1381-1393 (1967).
17. J. C. Mitchell and D. J. Meier, Journal of Polymer Science Part A-2-Polymer Physics 6, 1689-1703 (1968).
18. B. Huneau, Rubber Chem. Technol. 84 (3), 425-452 (2011).
19. N. Candau, L. Chazeau, J. M. Chenal, C. Gauthier, J. Ferreira, E. Munch and C. Rochas, Polymer 53 (13), 2540-2543 (2012).

20. P. A. Albouy, G. Guillier, D. Petermann, A. Vieyres, O. Sanseau and P. Sotta, Polymer 53 (15), 3313-3324 (2012).
21. M. Tosaka, K. Senoo, K. Sato, M. Noda and N. Ohta, Polymer 53 (3), 864-872 (2012).
22. K. Bruning, K. Schneider, S. V. Roth and G. Heinrich, Macromolecules 45 (19), 7914-7919 (2012).
23. N. Candau, R. Laghmach, L. Chazeau, J.-M. Chenal, C. Gauthier, T. Biben and E. Munch, Macromolecules 47 (16), 5815-5824 (2014).
24. N. Candau, R. Laghmach, L. Chazeau, J.-M. Chenal, C. Gauthier, T. Biben and E. Munch, Submitted to Polymer.
25. Rauline R. US. Patent, 5, 227, 425, (Michelin) (1993).
26. P. J. Flory and J. Rehner, J. Chem. Phys. 11 (11), 521-526 (1943).
27. P. A. Albouy, J. Marchal and J. Rault, Eur. Phys. J. E 17 (3), 247-259 (2005).
28. G. R. Mitchell, Polymer 25 (11), 1562-1572 (1984).
29. P. J. Flory, J. Chem. Phys. 15 (6), 397-408 (1947).
30. E. M. Arruda, M. C. Boyce. Journal of the Mechanics and Physics of Solids. 41 (2), 389-412 (1993).
31. J. R. S. Martinez, J. B. Le Cam, X. Balandraud, E. Toussaint and J. Caillard, Polymer 54 (11), 2727-2736 (2013).
32. J. R. S. Martinez, J. B. Le Cam, X. Balandraud, E. Toussaint and J. Caillard, Polymer 54 (11), 2717-2726 (2013).
33. E. H. Andrews, Proc. R. Soc. Lond. A-Math. Phys. Sci. 277 (1370), 562-570 (1964).
34. J. M. Chenal, L. Chazeau, Y. Bomal and C. Gauthier, J. Polym. Sci. Pt. B-Polym. Phys. 45 (8), 955-962 (2007).
35. P. J. Phillips and N. Vatansever, Macromolecules 20 (9), 2138-2146 (1987).

36. B. C. Edwards, J. Polym. Sci. Pt. B-Polym. Phys. 13 (7), 1387-1405 (1975).

37. L. H. Sperling, *Introduction to physical polymer science*. (Wiley. com, 2005).

38. H. G. Kim and Mandelkern.L, Journal of Polymer Science Part A-2-Polymer Physics 10 (6), 1125-1133 (1972).

39. E. N. Dalal, K. D. Taylor and P. J. Phillips, Polymer 24 (12), 1623-1630 (1983).

40. J. D. Hoffman, Davis, G. T., & Lauritzen Jr, J. I., *Treatise on Solid State Chemistry*. (New York, 1976).

41. H. M. James, E. Guth, J. Chem. Phys 11 (10), 455−481 (1943).

42. L. R. G. Treloar, The physics of rubber elasticity; Oxford: Oxford, U.K., (1975).

43. S. Toki, I. Sics, S. F. Ran, L. Z. Liu and B. S. Hsiao, Polymer 44 (19), 6003-6011 (2003).

44. M. Tosaka, Macromolecules 42 (16), 6166-6174 (2009).

45. M. L. Williams, R. F. Landel and J. D. Ferry, Journal of the American Chemical Society 77 (14), 3701-3707 (1955).

46. E. Munch, J.-M. Pelletier, B. Sixou and G. Vigier, Physical review letters 97 (20), 207801 (2006).

47. J. Carretero-Gonzalez, T. A. Ezquerra, S. Amnuaypornsri, S. Toki, R. Verdejo, A. Sanz, J. Sakdapipanich, B. S. Hsiao and M. A. Lopez-Manchado, Soft Matter 6 (15), 3636-3642 (2010).

48. K. Adachi and T. Kotaka, Macromolecules 18 (3), 466-472 (1985).

49. P. Rublon, Thesis, Ecole centrale de Nantes-ECN, Nantes, France, 2013.